DESIGN AND EXPERIMENT OF MULTI-PUROSE AND MODULAR SENSOR ROBOTIC PLATFORM FOR REAL-TIME ASSESSING AND MONITORING OF CEA FARMS USING POINT CLOUD, LIDAR, RGB AND THERMAL IMAGING
/
PROIECTAREA ȘI TESTAREA UNEI NOI SOLUȚII MULTI-SCOP DE PLATORMĂ SENZORIALĂ ROBOTICĂ PENTRU EVALUAREA FERMELOR DE TIP CEA UTILIZÂND TEHNOLOGII POINT-CLOUD, LIDAR, IMAGISTICĂ RGB ȘI TERMICĂ

Alexandru STAN[1)], Cosmin Karl BĂNICĂ[1)], Costin Hedwig GÂNDESCU[1)], Claudiu SIMION[1)], Diana-Maria COTOROBAI[1)], Valentin SIMION[1)] Cornelia MURARU-IONEL[2)],
[1)]LIGHTNING-NET SRL Bucharest/Romania;
[2)] INMA Bucharest/Romania
Tel +40742226193; E-mail: cmuraru@inma-ita.ro
DOI: https://doi.org/10.35633/inmateh-77-01

Keywords: *Agricultural and Industrial Systems, Controlled-Environment Agriculture Monitoring and Control, Flexible Robotic Platform, LiDAR, 2D mapping, RGB and Thermal Imaging, Volumetric Point-Cloud.*

ABSTRACT

*To address the challenges and needs of the CEA (Controlled Environment Agriculture) farms, a complex and multi-purpose sensor robotic platform was developed. The objective was to solve the problem of providing a complete set of visual and numeric information in regards to operational environment and specific points of interest within the environment. In this article, an experimental sensor robotic platform model was constructed and tested by integrating technologies such as LiDAR (*Light Detection and Ranging*) mapping via ROS (Robot Operating System), point-cloud, RGB and IR imaging and image processing algorithms developed with OpenCV (Open Computer Vision) libraries. Real-time control and environment assessment were achieved by integrating an internet access point within the structure of the experimental model. Experiments show that a multi-sensory integration and operation can be successfully achieved within a compact and energy efficient robotic platform, reaching six hours of autonomy The LiDAR-based experiments show that the proposed system can achieve a $\pm 7\ mm$ mapping precision, greatly enhancing the operation within the environment. Furthermore, the RGB, IR imaging, point-cloud and image processing algorithms proved to optimize the assessment and monitoring operations by providing valuable and precise visual information. The final results show that the proposed solution has great performance in controlled environments and can improve the safety and overall efficiency of CEA farms and related environments.*

REZUMAT

Pentru a răspunde provocărilor și nevoilor identificate în cadrul fermelor de tip CEA (Agricultura în mediu controlat) a fost dezvoltată o platformă senzorială robotică multi-scop. Obiectivul principal este a fost ca soluția propusă să ofere operatorilor un set complet de informații vizuale și numerice în raport cu mediul în care operează platforma robotică. În cadrul acestui articol, este prezentată proiectarea și testatarea unui model experimental de platformă senzorială integrând tehnologii de vârf, precum cartografiere 2D prin intermediul LiDAR și ROS, imagistică point-cloud, RGB și IR și algoritmi de procesare de imagine prin intermediul bibliotecilor software OpenCV. Prin conectarea platformei robotice la internet, este posibilă accesarea acesteia de la distanță și controlul și monitorizarea în timp real a mediului de operare. Încercările realizate indică faptul că operarea și implementarea unei varietăți de senzori pot fi integrate cu succes într-o platforma senzorială robotică compactă și eficientă energetic, prezentând o autonomie de până la șase ore. Încercările cu modulul LiDAR au dovedit faptul că sistemul are o precizie de cartografiere de $\pm 7\ mm$, îmbunătățind operarea în mediile vizate. În plus, imagistica RGB, IR, point cloud și algoritmii de procesare a imaginilor au dovedit faptul că îmbunătățesc considerabil operațiunile de monitorizare și evaluare prin furnizarea de informații vizuale de mare precizie. Rezultatul final arată faptul că soluția propusă prezintă performanțe ridicate în eficientizarea fermelor de tip CEA și a mediilor conexe.

[1] *Alexandru Stan, PhDs; Cosmin Karl Bănică, Assoc. Prof. PhD; Costin Hedwig Gândescu, PhD; Claudiu Simion, MSc.; Cornelia Muraru-Ionel, PhD; Diana-Maria Cotorobai, PhDs; Valentin Simion, MSc.*

INTRODUCTION

The need of modern robotic systems has dramatically increased since concepts like *Industry 4.0*, *Agriculture 4.0* and *Smart Farming* started to be integrated within all industrial branches. Thus, beneficiary entities demanded smart robotic systems to substitute and aid human operators in certain activities to enhance overall safety and efficiency within all agricultural and industrial environments and further promote the circular economy (*Adriny et al., 2015*). The growing need revolves around modular robotic systems capable of conducting various specific tasks and being able to accommodate a wide range of sensors and devices, such air quality sensors, RGB, IR and depth perception cameras, robotic arms and so on (*Pan et al., 2024; Gibb et al., 2017; Adriny et al., 2015; Rohmer et. al., 2013; Rjeb et al., 2021; Tai et al., 2024; Călinoiu, 2009; Wilson et al., 2023*). One of the most important challenges in mobile robotic platforms design, is detecting the environment configuration, the obstacles within and operating safely in close-quarters environments, such as storage warehouses, indoor farms, silos, greenhouses, farmyards (*Enoch et al., 2024; Ganduri et al., 2025; Javaid et al., 2022; Keith et al., 2024*). This is achieved by integrating state-of-the art LiDAR modules and depth perception cameras for real-time environment perception and assessment (*Blanco et al., 2010; Cadena et al., 2016; Campbell et al., 2020; De Huevel et al., 2024; Ardiny et al., 2015; Štepánová et al., 2018; Yu et al., 2021*). Furthermore, the existent and emergent technologies fused together under a modern and widely spread practice known as ***CEA farms*** – ***Controlled-environment agriculture***. CEA encompasses indoor farming and vertical farming, integrating a wide range of technologies, such as greenhouses, aeroponics, hydroponics, precision agriculture, vertical farming, plant science, robotics and so forth. By controlling the environmental variables, such temperature, light, carbon dioxide and the root-zone growing medium, the CEA farms can output healthy and constant production of edible, ornamental and high value plants (*Ojo et al., 2022; Cowan et al., 2022*). Therefore, CEA farms are engineered to provide optimal conditions for growing crops and prevent disease and pest damage (*Srivani et al., 2019*)

In order to achieve high standards of production and quality, the CEA farms must be equipped with state-of-the-art intelligent systems. For example, the project ***GROWx 2.0***, conducted by the AMS Institute (*Amsterdam Institute for Advanced Metropolitan Solutions*) aims to be a fully automated robotic vertical farm that is able to function in a closed-loop while optimizing every vital variable by using data from IoT sensors.

Furthermore, mobile robotic platforms also proved high utility within indoor and even and firm terrain farming environments, such as: farmyards, storage facilities and silos and greenhouses. Robotic mobile platforms are able to perform a wide range of applications within mentioned environments, such as: transporting and handling various CEA-specific items, conducting video crop inspections by using RGB, IR and multispectral cameras, harvesting operations, conducting LiDAR-based environment mapping, surveying mentioned environment variables and so forth. For example, *Harvest Automation* designed and deployed a mobile robotic platform, designated HV-100, effective within greenhouse, hoop house and nursery environments, and it is in charge with spacing and collection tasks, see Figure 1 and 2.

Fig. 1 – Harvest Automation – HV-100

Fig. 2 – Two HV-100 mobile robots in a nursery

An example of indoor harvesting robotic platform is **Virgo 1**, designed and deployed by Root AI to detect ripe small-sized fruit, for example: cherry tomatoes, strawberries, and harvest them without inflicting damage. This is achieved with the help of a robotic mobile platform carrying a robotic arm equipped with a stereoscopic camera and a custom designed gripper. **Virgo 1** uses intelligent image processing algorithms in order to detect and determine the ripeness of a fruit/vegetable in percentages based on the real-time captured images.

Fig. 3 – Virgo1 picking cherry tomatoes

Fig. 4 – Virgo1 – gripper detailed view

Fig. 5 – Virgo1 picking strawberries

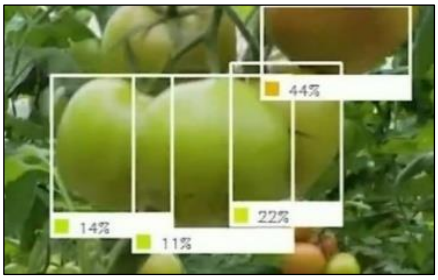

Fig. 6 – Virgo1 fruit/vegetable ripeness detection

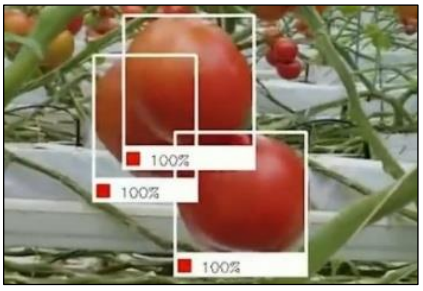

Fig. 7 – Virgo1 fruit/vegetable ripeness detection

In order to be efficient and able to carry a wide variety of CEA specific tasks, mobile robotic platform designed for CEA applications, is mandatory to accommodate the following hardware and software configuration *(Siciliano et al., 2016)*: LiDAR Module, stereoscopic camera, IR or multispectral camera, drive-wheels, proximity sensors, on-board computer, power distribution board, motherboard and power source, image processing algorithms.

MATERIALS AND METHODS

Design concept and structure

The authors of this paper propose a multi-purpose, retrofittable and Internet-teleoperated mobile robotic platform presenting a compact form-factor body and high modularity character in order to accommodate a wide spectrum of additional equipment, thus being able to conduct a broad variety of specific tasks in various domains, such as: industrial, energy and indoor agriculture environments. The main aim for the robotic platform is to operate within CEA environments and perform specific tasks. Therefore, the proposed solution can accommodate supplementary equipment, such as thermal imaging cameras, sound capturing equipment, robotic arms, visible spectrum cameras, gas-leak detectors, medical equipment and many more. Being able to integrate visible and invisible spectrum cameras, the robotic platform can be used to monitor crop health, detecting diseases, pest infestations, or nutrient deficiencies. In addition to this, the solution can also monitor the integrity of the equipment found in CEA environments, such as electrical panels, solar inverters, and so on. Moreover, integrating dedicated sensors and equipment, environment parameters, such as ambient temperature, humidity and gases, can be surveyed in real time.

Structure-wise, authors developed a lightweight, modular and easy-to-assemble frame. The BOSCH extruded aluminum profile rendered to be the most suitable solution. Regarding locomotion, authors implemented a simple configuration integrating two drive-wheels and two support omnidirectional wheels symmetrically along the sagittal and frontal planes, as shown in Fig.8. This decision was made in order for the robotic platform to be able to perform maneuvers and navigate in close-quarters spaces, such as vertical farming and greenhouse environments.

Furthermore, the authors developed and integrated a modular and 3D printed outer shell by using magnetic coupling. By doing so, operators can replace damaged plates without disassembling the entire shell assembly. In addition to this, depending on the working environment, operators can 3D print the outer-shell using various technical thermoplastics, thus obtaining hard or soft outer-shell. Regarding electronics, authors integrated a custom-made motherboard and mandatory opto-electronic devices, sensors and processing units. The mobile robotic platform has an Ubuntu computer integrated and it is aided by a pair of microcontrollers to process the low-level sensors and peripherals, such as status LEDs, cooling fans and so on. The final design concept and structure is presented in the following CAD images:

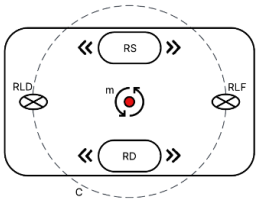

Fig. 8 – Locomotion concept of the proposed mobile robotic platform

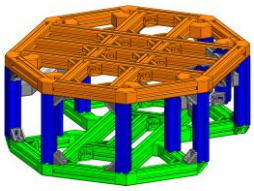

Fig.9 – CAD structural frame
Orange – Top frame layer;
Blue – Support columns;
Green – Bottom frame layer

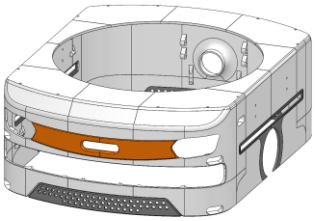

Fig. 10 – Modular 3D prototyped shell

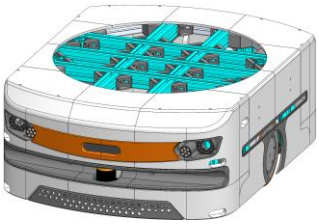

Fig. 11 – Final design concept – CAD view

As previously stated, the extruded aluminum BOSCH profile, with cross-section $l_{\square} = 30mm$, was chosen for the structural frame of the mobile robotic platform due to the lightweight and mechanical characteristic of aluminum. The structural concept of the frame encompasses a top layer, support columns and a bottom layer, all inter-assembled by nuts and bolts. As previously illustrated, the structural frame consists of two main components, the top and bottom, vertical interfacing beams. In order to validate de design, a FEA is conducted by using *Solidworks Simulation* to determine the safety factor of entire frame regarding compression stress. The red marked surfaces in Figure.12 represent the contact surfaces of the distributed and axial compression stress to the frame, whereas the green marked surfaces represent fixed surfaces, simulating the drive-wheels reaction force to the axial compression force. For the simulation, the chosen compression force is $F_c = 800N$. Fig.14 shows that the overall stress gradient resides mostly within the blue region, denoting very low stress induced areas. Moreover, the maximum stress resulted in the structural frame according to the FEA is $\sigma_s = 19{,}7\ MPa$.

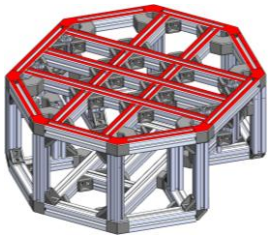

Fig. 12 – CAD metal frame

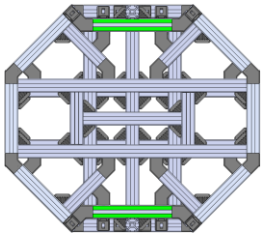

Fig. 13 – CAD metal frame – bottom view

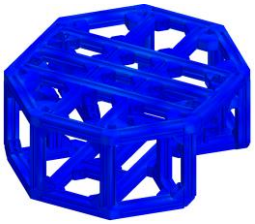

Fig. 14 – CAD structural frame
Post-FEA simulation

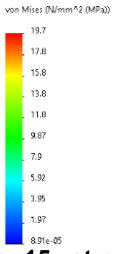

Fig. 15 –stress gradient

Considering that the maximum tensile strength of the aluminum used in BOSCH profiles according to Bosch Rexroth is $\sigma_{max} = 200\ N/mm^2 = 200\ MPa$ the safety factor can be calculated using the following equation:

$$SF = \frac{\sigma_{max}}{\sigma_s} = \frac{200\ MPa}{19.7\ MPa} = 10.15 \quad (1)$$

As it is shown in equation (1), the safety factor is $SF = 10.15$, meaning that the frame can withstand, theoretically, to an axial compressive force up to $F_{max} = 8000N$.

Sensor and peripherals

The mandatory sensorial peripherals required to be integrated within the robotic platform in order to perform accordingly are a LiDAR module, an RGB-depth perception camera and a thermal imaging camera. The authors have chosen the Hokuyo UST-10LX industrial-grade LiDAR, Intel RealSense D435i RGB-depth perception camera and thermal imaging camera Viewpro A40T due to the great capabilities and the small form factor. In order to successfully integrate the thermal imaging camera, Viewpro A40T, a metal interfacing structure was needed. Operators are able to observe the real-time thermal imaging results by using the portable screen mounted on the interfacing structure. The next figures present the interfacing assemblies and integrated sensorial peripherals.

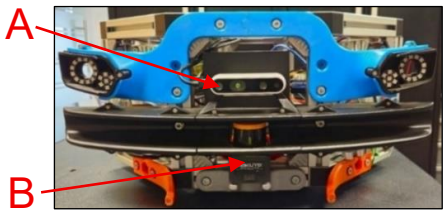

Fig. 16 – Camera (A), LiDAR (B) and headlights mounted

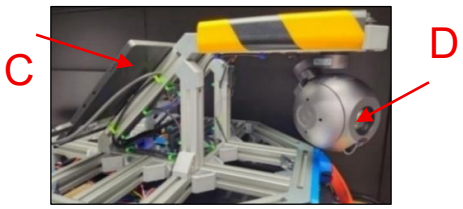

Fig. 17 – Thermal imaging assembly; Portable screen (C) and Viewpro A40T (D)

Bodywork design

Authors designed the outer-shell to cover a range of functional aspects as follows: offer protection against harsh environments, allows *hot-swapping* plates in case of damage and provide commercial aspect. The chosen manufacture method is rapid prototyping via FDM technology. By doing so, manufacture time and costs are greatly reduced. In order to manufacture the outer shell, the entire assembly had to be split in three large assemblies and split further into smaller elements. Having the front, rear bumper and lateral panels divided into smaller individual panels, they can be 3D printed and then assembled via nuts and bolts where is the case. The resulted elements and assemblies are presented in the next figures:

Fig. 18 – Front bumper

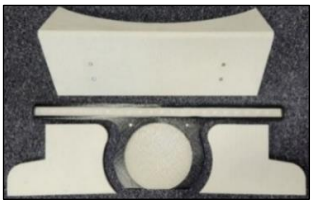

Fig. 19 – Lateral panel

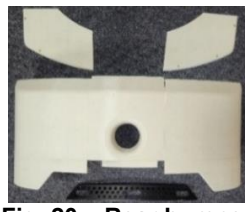

Fig. 20 – Rear bumper

Robotic platform assembly

Next, considering all the presented above, the final assembly of the robotic platform is presented in the images below. The assembly process consists of cabling and wire-management, installing the motherboard and installing the modular bodywork.

Fig. 21 – Installed and powered-up motherboard

Fig. 22 – Robotic platform – complete assembly

Integration of additional sensors and electronic devices

During the design stage of the robotic platform, it has been decided that the top layer of the frame will serve also as a mounting base for allowing the integration of additional sensorial devices and equipment. By doing so, depending on the operating environment and needs, the robotic platform can be equipped with a wide range of additional equipment, as presented in the next figure:

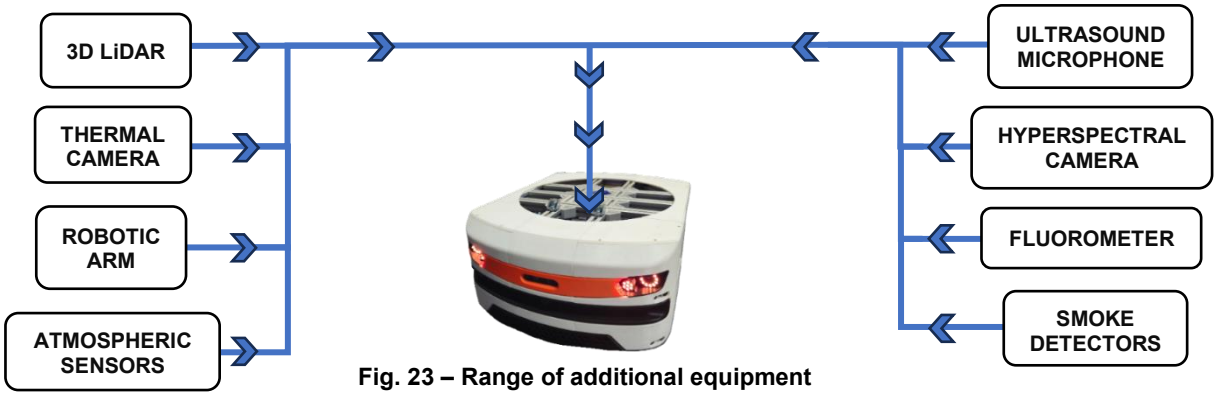

Fig. 23 – Range of additional equipment

By being able to integrate such a wide range of additional equipment represents a major advantage. Thus, the robotic platform becomes an indispensable universal work-frame ready to serve in numerous agricultural applications and industrial environments with ease. The importance of serving as multi-purpose base-frame for numerous agricultural environments is marked by the possibility of integrating and combining the functions of various sensorial equipment in order to perform a wide range of tasks. For example, RGB cameras can be used for determining plant properties, such as color, morphology, biomass, leaf area and leaf movement. Furthermore, a thermal camera can determine another set of plant parameters, such as organ temperature, transpiration and stomatal conductance and also surveying growth environment state. Moreover, LiDAR allows operators to bidimensional map the area of operation and also teleoperate in safe conditions, being able to observe obstacles and navigate by the culture and crop beds, equipment and personnel.

Methods of experimental validation

In order to validate the operating concept and function of the developed experimental model, several tests were performed indoors in regards to RGB and thermal imaging, point-cloud generation, LiDAR 2D environment mapping and image processing algorithms. Authors tested the thermal imaging capabilities in production and storage warehouse containing power lines, electric panel, solar inverters and wireless transmission devices, equipment that is also found in CEA farms. The RGB imaging, including image processing algorithms were tested indoors, in controlled environment. In regards to point-cloud generation, the authors conducted indoor testing point-clouds to generate vegetation canopy and operating environment point-clouds. For the experimental validation of the indoor 2D mapping of the operational environment and obstacles detection, authors used the on-board LiDAR, the Hokuyo 10LX, in order to simulate the close-quarters environments found in greenhouses and indoor vertical farms.

RESULTS

Accessing and operating method

Authors integrated a simple, yet efficient teleoperating solution via internet. By integrating an on-board computer with a wi-fi module included, the robotic mobile platform can access and be accessed via internet on-site. In the case internet is not available on-site, the robotic platform can be equipped with a USB modem or even a ***STARLINK*** receiver for uninterrupted and world-wide internet access. By having internet connection, the robotic platform can be accessed through the *Remote Desktop Connection* function of, for example, a laptop, and interact in real-time. This method greatly improves the ease of access of the robotic platform and offers great flexibility regarding operating the robotic platform in various environments without being dependent of the on-site internet source. Furthermore, operators can run remotely the developed software routines, such as bidimensional environment map generation, volumetric data points generation, visual processing algorithms, control and so on. The mentioned routines were developed by the authors using *Python* programming language on an Ubuntu OS machine in the *ROS – Robot Operating System work environment*. The algorithms are run and data is processed on the Ubuntu machine integrated within the experimental model. The access and control concept is presented in the following diagram.

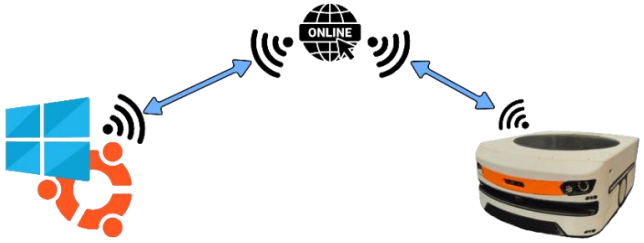

Fig. 24 – Accessing and control concept between a control computer and robotic platform via internet

Bidimensional LiDAR mapping via RVIZ

Authors performed a variety of tests regarding the precision of bidimensional mapping of the Hokuyo 10LX LiDAR. Data acquisition and 2D map generation is performed by *Robot Operating System Visualization* software, ***RVIZ***. RVIZ is an open-source software that allows operators to visualize in real-time numerical data transmitted by the robotic platform. As previously stated, the Hokuyo 10LX is an industrial-grade LiDAR with a $\pm 40mm$ precision and $< 30mm$ repeatability. The precision was tested in laboratory conditions by placing the robotic platform relatively close to a wall and measuring the distance using the LiDAR.

Firstly, the placement distance relative to the wall was measured via a tape ruler, see Figure 25. In Figure 26, the red vertical axis represents the rotational axis of the LiDAR's oscillating mirror and it intersects the tape ruler at $d_{lid} = 1035\ mm$. Thus, the relative distance of the robotic platform to the wall, having as reference the LiDAR, is $d_{lid} = 1035\ mm$.

Fig. 25 – Testing LiDAR accuracy via tape ruler

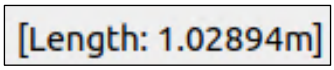

Fig. 28 – RViz screenshot of real-time length measurement

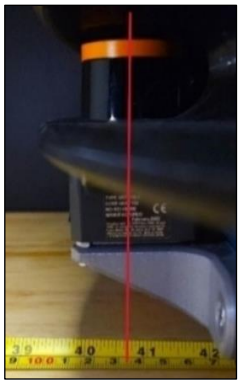

Fig. 26 – LiDAR accuracy validation

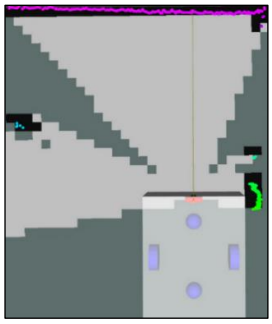

Fig. 27 – RViz screenshot of real-time visualization and distance measuring

In Figure 27, respectively Figure 28, authors presented two screenshots from RVIZ, regarding real-time distance measurement. Therefore, in Figure 27, the relative distance from the LiDAR to the wall is marked by the dark-yellow line, and the measured distance is presented in Figure 28, $d_{mes} = 1.029\ m = 1028\ mm$. Therefore, the measurement error is represented by Δl as follows:

$$\Delta d = d_{mes} - d_{lid} \tag{2}$$

$$\Delta d = (1028 - 1035)\ mm$$

$$\Delta d = -7\ mm \tag{3}$$

From (3) it is shown that the measurement error is $\Delta d = -7mm$, which is acceptable given the fact that the stated precision by the manufacturer is $P = \pm 40mm$.

Next, authors conducted a bidimensional mapping test in order to validate the mapping function and the ability to teleoperate the robotic platform in a close-quarters environment based on the LiDAR information. Furthermore, a simplified 3D model was integrated within *RViz* in order to reflect the real-time operation. The dimensions of the 3D model are in conformity with the ones of the real robotic platform, $720mm \times 520mm \times 235mm$. Next, various obstacles were placed within the testing environment in order to teleoperate around them and also mark them in the bidimensional map generated in real-time by Rviz. In the following images, the 2D cartography process is presented by showing the real-time data acquisition and bidimensional map generation of a close-quarters building floor. The robotic platform is represented by the green parallelogram. The first obstacles are a battery charger and a compressor. The obstacles appear in the figures below marked with a yellow circle for the air compressor and red circle for the battery charger.

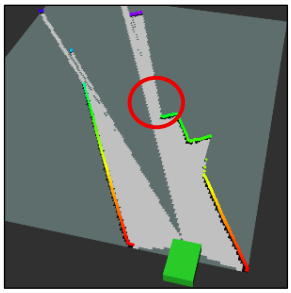

Fig. 29 – Mapping process started. First object – Red circle

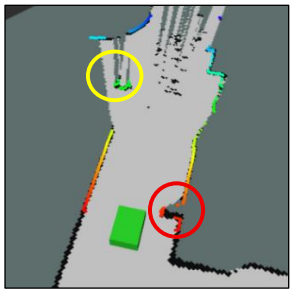

Fig. 30 – Obstacles observed by the LiDAR.

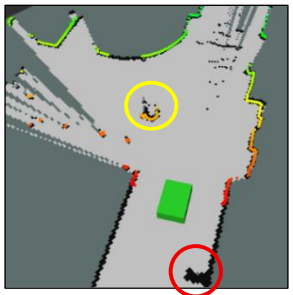

Fig. 31 – Mapping proceeds

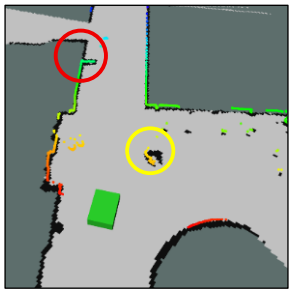

Fig. 32 – Robotic platform on the way to the starting point

Next, as previously stated, Rviz is able to save a 2D map after the mapping procedure has been completed. The 2D map based on the LiDAR data collected for the testing purpose **was generated in real-time** during the motion of the robotic platform. Essentially, no post-processing actions are needed in order to obtain a map of the environment. The 2D generated map is presented in the following image:

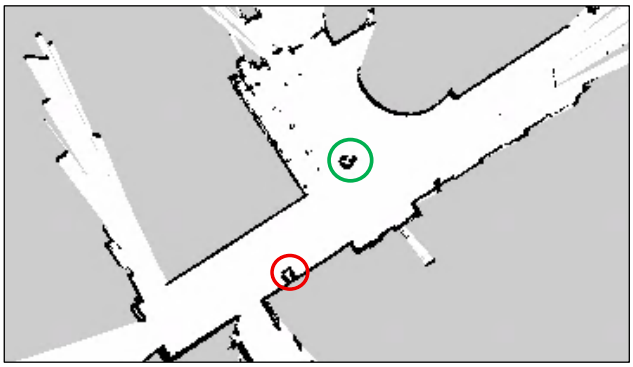

Fig. 33 – 2D map generated by RViz based on LiDAR data
Green circle – obstacle 1 (air compressor); Red circle – obstacle (battery charger)

Volumetric point-clouds

By using the on-board depth-perception camera, the Intel D435i, the authors were able to generate volumetric cloud-points for plants canopy and environment in real-time. Authors performed a series of tests in order visualize the process. The test was performed in a controlled environment, where the lighting conditions are constant. By running the cloud-point generation algorithm, a virtual representation of the observed environment was constructed in real-time within RViz and in scale with the simplified 3D model of the robotic platform. In the next figures, the real-time result is presented from a 3rd person and dimetric perspective.

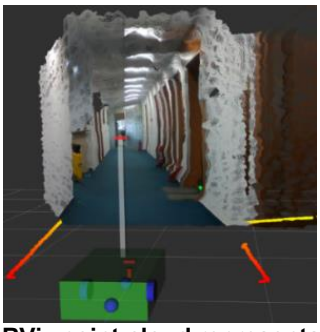

Fig. 34 – RViz point-cloud representation – 3rd person perspective

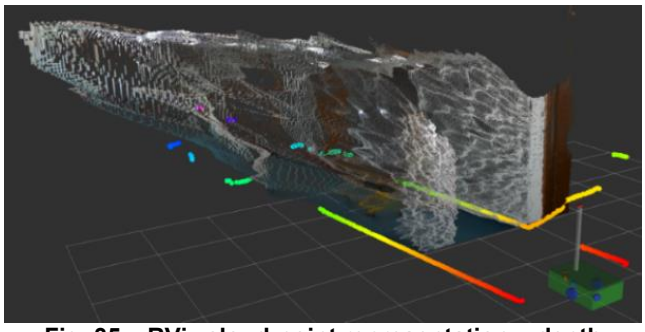

Fig. 35 – RViz cloud-point representation – depth perspective

Next, the same testing method was performed, but capturing various plants types as follows:

Fig. 36 – RGB image capture by the stereoscopic camera for plant no. 1

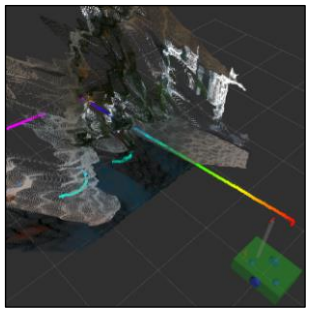

Fig. 37 – Point-cloud representation – depth perspective

Fig. 38 – RGB image capture by the stereoscopic camera for plant no. 2

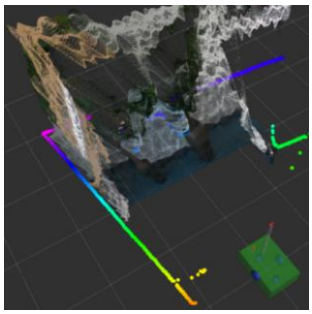

Fig. 39 – Point-cloud representation – 3rd person perspective

Image processing algorithm

By using an image processing algorithm, operators were able to detect plants by extracting the specific colors. Furthermore, this algorithm is also usable for detecting affected areas in leaves, such as brown spots. For testing purposes, authors developed a color extraction algorithm. In order to accurately extract the green color, authors converted the images from the RGB color space to HSV color space. The HSV color space allows a more precise color extraction, due to its three main parameters: Hue, Saturation and Value.

The algorithm was developed using Python programming language and the ***OpenCV*** image processing software library. In following figures, the color extraction process is illustrated for the following plants.

Fig. 40 – RGB image of plant no.1

Fig. 41 – Transition to HSV color space

Fig.42 – HSV mask applied for color extraction

Fig.43 – RGB result of plant extraction

In order to provide additional information about the original image, Figure 40, such as tonal distribution, a histogram plot for each image was generated as follows:

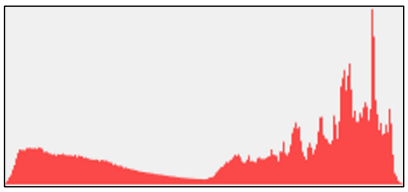

Fig. 44 – Histogram red channel

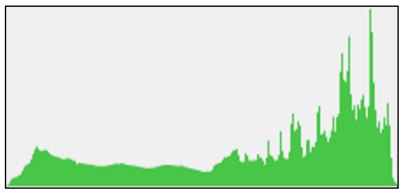

Fig. 45 – Histogram green channel

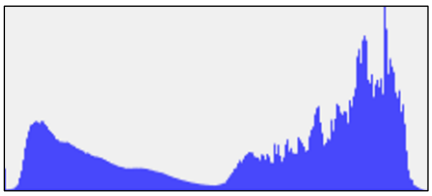

Fig. 46 – Histogram blue channel

Regarding brown spots detection, an image of an affected leaf from the plant in Figure 67 was taken in order to test the algorithm. The algorithm will detect the contour of the leaf, calculate the area within the exterior of the contour and subtract the area of the affected zones in order to calculate the relative percentage of healthy leaf.

Fig.47 – Entire leaf image

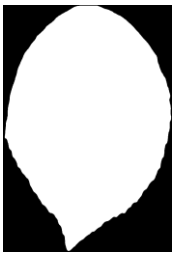

Fig.48 – Binary image of the leaf for contour extraction

Fig.49 – Contour (magenta) with original image overlay

Fig.50 – Binary image of the affected areas for contour extraction

Fig.51 – Contour (magenta) with original image overlay

The area within the contour in Fig.49 is approximately $A_T = 566{,}724\ px^2$, and the affected areas in Fig. 51 have a total of $A_D = 79{,}704\ px^2$. By subtracting the damaged area from the total area of the leaf, the percentage of healthy surface, A_H can be calculated. Therefore:

$$A_H = A_T - A_H \tag{4}$$

$$A_H = (566{,}724 - 79{,}724)\ px^2$$

$$A_H = 487{,}522\ px^2 \tag{5}$$

From (5) the surface area of the healthy portion of the leaf is $A_H = 487{,}522\ px^2$. Converting the A_H to the percentage relative to the entire leaf area, 85.9% represents the healthy surface of the leaf and 14.1% represents the total affected area.

Thermal imaging

Authors performed a series of experiments with the on-board thermal camera in a warehouse containing various equipment and energy converters also found in CEA environments.

The results of the thermal imaging are presented in the next figures. The images are screenshots taken from the dedicated IR camera software. Moreover, the results are illustrated in PIP mode (Picture-In-Picture). Therefore, the RGB images are placed in the foreground of the entire image as follows:

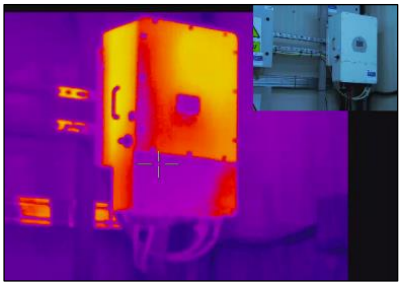

Fig. 52 – Thermal imaging of a solar inverter

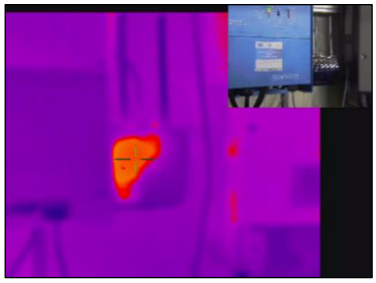

Fig. 53 – Thermal imaging of a communication device

Fig. 54 – Thermal imaging of an electric panel

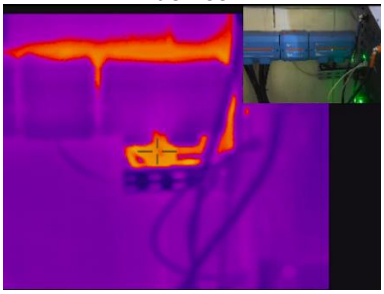

Fig. 55 – Thermal imaging of rails and power lines

Autonomy bench-testing

The robotic platform is designed to run on two *6s – 25.2 VDC* LiPo batteries, *16000mAh* capacity per battery, batteries connected in parallel. By doing so, robotic platform has a grand total of $P_t = 806/4W$ of electrical power available. Knowing that the average consumption of the robotic platform is $I_{av} = 5A$, it can be determined through calculus the maximum autonomy is $A_{max} = 6\ h\ 24\ min$. This can be verified by connecting the two LiPo batteries to a programmable DC electronic load and set a continuous amperage draw of $5A$. In order to simplify the laboratory test, only one LiPo battery will be connected to the electronic load. In order to obtain the numerical data of the discharge process, the electronic load is connected via USB cable to a laptop. Next, the discharge characteristic is presented in the next figure:

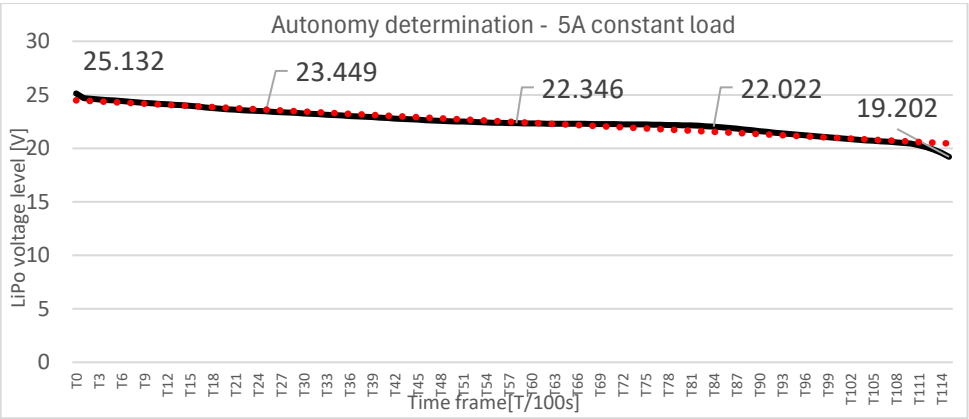

Fig. 56 – LiPo discharge characteristic

Fig.57 – Bench testing setup

Down – Electronic load; Up – Tattu Plus 16000 mAh LiPO

T_0 represents the initial moment of the discharge process. The sampling rate of the data is $f = 0{,}01Hz$. From the figure above it is shown that the LiPo battery will get from a full charge state, *25.2 VDC* and to the discharged state, *19.2 VDC,* in approximately 3 hours and 12 minutes. Therefore, by connecting two LiPo batteries in parallel, the **autonomy doubles to 6 hours and 24 minutes.**

CONCLUSIONS

(1) The authors of this paper designed, manufactured and tested a new robotic platform in a compact form-factor that can be used in CEA farms and in wide range of additional environments. For example, it is well suited for transporting loads in industrial warehouses, grain storages, greenhouses, CEA farms and so on. Furthermore, the mobile robotic platform can also serve as a universal sensorial platform for specific applications by allowing a wide variety of equipment to be mounted on not only for agricultural tasks, but industrial also. For example, additional sensors, RGB, IR and multispectral imaging cameras, specialized microphones and robotic arms can enhance the capabilities of the proposed robotic platform solution.

(2) The metal frame was designed in such manner that it allows modularity and flexibility regarding the addition of sensorial devices. Furthermore, based on the FEA CAD simulation, the frame can withstand heavy loads, ranging from $m_{norm} = 80kg$, to $m_{max} = 800kg$, having a safety factor value of $SF = 10.15$.

(3) Designing the outer shell of the mobile robotic platform was also a key factor in the overall development of the presented solution. Authors developed a functional and commercially appealing outer shell. Thus, the outer shell can be manufactured by using rapid prototyping technologies and it can be mounted to the frame by magnetic coupling. By doing so, the solution is modular, and the protective plates can be *hot swapped* in case of damage or any other reason. The outer shell can also be replaced as a whole if the conditions and needs of the operational environment require so.

(4) Authors successfully performed thermal imaging experiments that validated the functionality and utility of such feature within CEA farms and related environments. The developed image processing algorithms were successfully tested for detecting plants' canopy, biomass and affected areas.

(5) The real-time environment assessment technologies proved to work faultlessly in the testing stages in a whole and functional system. Therefore, the authors successfully mapped in real-time the testing environment with the LiDAR module and generated a partial point-cloud of the test plants' canopy and environment.

(6) The presented multi-purpose hybrid robotic platform has an outstanding potential within CEA and adjacent environments due to the design concept and flexibility. Being able to integrate and combining sensorial and mechatronic equipment greatly contributes to increasing efficiency and safety other industrial environments, such as automotive, aerospace, photovoltaic, and power plants.

ACKNOWLEDGEMENT

This paper was developed within the program "Autonomous polymorphic robotic platforms for service systems within Smart City (ProSSSy)" - SMIS No. 121220, Contract No. 255/ 05.06.2020.

REFERENCES

[1] Akbari, M., (2023). Revolutionizing supply chain and circular economy with edge computing: Systematic review, research themes and future directions. *Management Decision*. https://doi.org/10.1108/MD-03-2023-0412

[2] Ardiny H., Witwicki S., Mondada F. (2015). *Construction Automation with Autonomous Mobile Robots: A Review. 3rd RSI International Conference on Robotics and Mechatronics (ICROM).* https://doi.org/10.1109/ISCID52796.2021.00037

[3] Ardiny H., Witwicki S., Mondada F (2015). "Autonomous Construction of Separated Artifacts by Mobile Robots using SLAM and Stigmergy," in *Conference on Autonomous and Robotic Construction of Infrastructure*.

[4] Blanco, J.L.; Gonzalez, J.; Fernandez-Madrigal (2010). J.A. Optimal Filtering for Non-parametric Observation Models: Applications to Localization and SLAM. *Int. J. Robot. Res.*, *29*, 1726–1742. https://doi.org/10.1177/0278364910364165

[5] Cadena C., Carlone L., Carrillo H., Latif Y., Scaramuzza D., Neira J., Reid I., Leonard J.J. (2016). Past, Present, and Future of Simultaneous Localization and Mapping: Toward the Robust-Perception Age. *IEEE Trans. Robot.*, *32*, 1309–1332.https://doi.org/10.48550/arXiv.1606.05830

[6] Călinoiu, Constantin (2009). *Sensors and Transducers (*Ro*: "Senzori și Traductoare"*), Vol.1, Bucharest, The Technical Press House.

[7] Campbell, S., O'Mahony, N., Carvalho, A., Krpalkova, L., Riordan, D., Walsh, J. (2020). Path planning techniques for mobile robots a review. In: *6th International Conference on Mechatronics and Robotics Engineering (ICMRE)*, pp. 12–16.https://doi.org/10.1109/ICMRE49073.2020.9065187

[8] Cowan N., Ferrier L., Spears B. M., Drewer J., Reay D., Skiba U., (2022). "*CEA Systems: the Means to Achieve Future Food Security and Environmental Sustainability?"* Frontiers Media. https://doi.org/10.3389/fsufs.2022.891256

[9] De Heuvel, J.; Zeng, X.; Shi, W.; Sethuraman, T.; Bennewitz, M. (2024). Spatiotemporal Attention Enhances Lidar-Based Robot Navigation in Dynamic Environments. *IEEE Robot. Autom. Lett.*, *9*, 4202–4209. https://doi.org/10.48550/arXiv.2310.19670

[10] Enoch O.S., Uchenna J.U., Olukunle O.A. and Akoh. A. (2024). AI-driven warehouse automation: A comprehensive review of systems. *GSC Advanced Research and Reviews*. 18. 272-282. 10.30574/gscarr.2024.18.2.0063.https://doi.org/10.30574/gscarr.2024.18.2.0063

[11] Ganduri, Krishnavamshi & Pathri, Bhargav & Rathod, Shivaji & Koganti, Sojith & Yanna, Kusuma & Reddy, Bakka & Pudi, Praveen Kumar. (2025). Adaptive Intelligence in Warehouse Robotics: Efficient Pick-and-Place Robot for Dynamic Environments. *Journal of Electrical Systems*. 8215-8230. https://doi.org/10.52783/JES.7892

[12] Gibb, S., Le, T., La, H.M., Schmid, R., Berendsen, T. (2017). A multi-functional inspection robot for civil infrastructure evaluation and maintenance. In: *IEEE/RSJ International Conference on Intelligent Robots and Systems (IROS)*, pp. 2672–2677.https://doi.org/10.1109/IROS.2017.8206091

[13] Javaid, M., Haleem, A., Singh, R.P. and Suman, R. (2022). Artificial intelligence applications for industry 4.0: A literature-based study. *Journal of Industrial Integration and Management*, 7(01), pp.83-111. https://doi.org/10.1142/S2424862221300040

[14] Keith, Russell & La, Hung. (2024). *Review of Autonomous Mobile Robots for the Warehouse Environment*. https://doi.org/10.48550/arXiv.2406.08333

[15] Ojo M. O., Zahid A. (2022). *Deep Learning in Controlled Environment Agriculture: A Review of Recent Advancements, Challenges and Prospects*, Multidisciplinary Digital Publishing Institute. https://doi.org/10.3390/s22207965

[16] Pan, Qiran. (2024). Design and analysis of an autonomous warehouse robot system with 6-DOF manipulator. *Applied and Computational Engineering*. 34. 114-121. https://doi.org/10.54254/2755-2721/34/20230310.

[17] Rohmer, Eric, Surya P. N. Singh, and Marc Freese. (2013). CoppeliaSim (formerly V- REP): A Versatile and Scalable Robot Simulation Framework. In *Proceedings of the 2013 IEEE/RSJ International Conference on Intelligent Robots and Systems*. New York: IEEE.

[18] Rjeb, A., Gayon, J.-P., Norre, S. (2021). Sizing of a heterogeneous fleet of robots in a logistics warehouse. In: *IEEE 17th International Conference on Automation Science and Engineering (CASE),* pp. 95–100. https://doi.org/10.1109/CASE49439.2021.9551422 . ISSN: 2161-8089

[19] Štepánová, K., Frederico B. K., Angelo C., and Michal V. (2018). "Mapping Language to Vision in a Real- World Robotic Scenario." *IEEE Transactions on Cognitive and Developmental Systems*. 10 (3): 784–794. https://doi.org/10.1109/TCDS.2018.2819359

[20] Siciliano B., Khatib O. (2016). *Springer Handbook of Robotics* 2nd Edition; Springer Handbooks: Berlin/Heidelberg, Germany;

[21] Srivani P., Y. D. C., Manjula S., (2019). A Controlled Environment Agriculture with Hydroponics: Variants, Parameters, Methodologies and Challenges for Smart Farming, *Fifteenth International Conference on Information Processing (ICINPRO)*. https://doi.org/10.1109/icinpro47689.2019.9092043

[22] Tai, Junjie. (2024). A design of intelligent AGV system combined with a robotic arm for flexible production lines. *Applied and Computational Engineering*. 34. 84-94. https://doi.org/10.54254/2755-2721/34/20230304

[23] Yu, N., Li, T., Wang, B. (2021). Multi-load AGVs scheduling algorithm in automated sorting warehouse. In: *14th International Symposium on Computational Intelligence and Design (ISCID)*, pp. 126–129. https://doi.org/10.1109/ISCID52796.2021.00037 . ISSN: 2473-3547

[24] Wilson, A & Gupta, Khushi & Koduru, Balu Harshavardan & Kumar, Abhinav & Jha, Ajit & Cenkeramaddi, Linga Reddy. (2023). Recent Advances in Thermal Imaging and its Applications Using Machine Learning: A Review. *IEEE Sensors Journal*. pp.1-1. https://doi.org/10.1109/JSEN.2023.3234335